Electronic nematic phase transition in the presence of anisotropy

Hiroyuki Yamase
Max-Planck-Institut für Festkörperforschung, Heisenbergstrasse 1, D-70569 Stuttgart, Germany
and National Institute for Materials Science, Tsukuba 305-0047, Japan
(Received 5 March 2014; revised manuscript received 29 April 2015; published 13 May 2015)

We study the phase diagram of electronic nematic instability in the presence of xy anisotropy. While a second-order transition cannot occur in this case, mean-field theory predicts that a first-order transition occurs near Van Hove filling and its phase boundary forms a wing structure, which we term a Griffiths wing, referring to his original work of He^3-He^4 mixtures. When crossing the wing, the anisotropy of the electronic system exhibits a discontinuous change, leading to a metanematic transition, i.e., the analog to a metamagnetic transition in a magnetic system. The upper edge of the wing corresponds to a critical end line. It shows a nonmonotonic temperature dependence as a function of the external anisotropy and vanishes at a quantum critical end point for a strong anisotropy. The mean-field phase diagram is found to be very sensitive to fluctuations of the nematic order parameter, yielding a topologically different phase diagram. The Griffiths wing is broken into two pieces. A tiny wing appears close to zero anisotropy and the other is realized for a strong anisotropy. Consequently three quantum critical end points are realized. We discuss that these results can be related to various materials including a cold atom system.

DOI: 10.1103/PhysRevB.91.195121 PACS number(s): 05.30.Fk, 64.70.Tg, 71.10.Hf, 71.18.+y

I. INTRODUCTION

Nematic liquid crystals are well known. Rodlike molecules flow like a liquid, but are always oriented to a certain direction in the nematic phase. This state is characterized by breaking of the orientational symmetry, retaining the other symmetries of the system. Electrons are point particles, not molecules. Nevertheless electronic analogs of the nematic liquid crystals were observed in a number of interacting electron systems: Two-dimensional electron gases [1,2], high-temperature superconductors of cuprates [3,4] and pnictides [5], the bilayer strontium ruthenate $Sr_3Ru_2O_7$ [6], and an actinide material URu_2Si_2 [7].

The electronic nematic order couples directly to an external anisotropy, which is thus expected to play a crucial role in a system exhibiting nematicity. The external anisotropy can be controlled by applying a uniaxial pressure, (epitaxial) strain, and sometimes by a crystal structure due to orthorhombicity. While it is generally not easy to quantify how much anisotropy is imposed on a sample, the anisotropy was calibrated recently by exploiting the piezoelectric effect [8]. A nematic susceptibility was then extracted and its divergence was demonstrated near a nematic critical point.

Encouraged by the experimental progress to control the external anisotropy, we study a role of the external anisotropy for the electronic nematic instability. This fundamental issue has not been well addressed even in mean-field theory. In particular, we focus on the nematicity associated with a d-wave Pomeranchuk instability (dPI) [9,10]. In a mean-field theory in the absence of anisotropy [11,12], the dPI occurs around Van Hove filling with a dome-shaped transition line. The transition is of second order at high temperatures and changes to first order at low temperatures. The end points of the second-order line are tricritical points.

The presence of a tricritical point (TCP) implies a wing structure when a conjugate field to the corresponding order parameter is applied to the system. This insight originates from the study of He^3-He^4 mixtures by Griffiths [13]. However, the conjugate field to the superfluid order parameter is not accessible in experiments. The wing structure predicted by Griffiths, which we term the Griffiths wing, was not tested for He^3-He^4 mixtures.

It was found that itinerant ferromagnetism occurs generally via a first-order transition at low temperatures and a second-order one at high temperatures [14]. The end point of the second-order line is a TCP. The order parameter is magnetization and its conjugate field is a magnetic field in that case. Similar to Griffiths's work [13], a wing structure emerges from the first-order transition line and extends to the side of a finite magnetic field. When crossing the wing, the system exhibits a jump of the magnetization, leading to a metamagnetic transition. Recently, the Griffiths wings were clearly observed in ferromagnetic metals such as UGe_2 [15] and UCoAl [16].

Given that TCPs are present in a mean-field phase diagram of the dPI [11,12], we may expect Griffiths wings also in an electronic nematic phase transition. Motivated by such insight, we explore possible Griffiths wings by studying a low-energy effective model of the dPI. A conjugate field to the nematic order parameter is xy anisotropy, which is accessible in experiments. By applying the anisotropy, we obtain a wing structure. However, in contrast to previous studies [13,14], the Griffiths wing exhibits a nonmonotonic temperature dependence. Furthermore we find that the wing structure is very sensitive to fluctuations of the order parameter, leading to a phase diagram topologically different from the mean-field result. These results can be related to various materials including a cold atom system.

II. MODEL

We study electronic nematicity associated with the dPI in the presence of xy anisotropy. Our minimal model reads

$$H=\sum_{\mathbf{k},\sigma}\left(\epsilon^0_{\mathbf{k}}-\mu\right)c^\dagger_{\mathbf{k}\sigma}c_{\mathbf{k}\sigma}-\frac{1}{2N}\sum_{\mathbf{q}}g(\mathbf{q})n_d(\mathbf{q})n_d(-\mathbf{q})-\mu_d n_d(\mathbf{0}), \quad (1)$$

where $c^\dagger_{\mathbf{k}\sigma}$ ($c_{\mathbf{k}\sigma}$) is the creation (annihilation) operator of electrons with momentum $\mathbf{k}$ and spin σ, μ is the chemical potential, and N is the number of sites. The kinetic energy $\epsilon^0_{\mathbf{k}}$ is given by a usual tight-binding dispersion on a square lattice,

$$\epsilon^0_{\mathbf{k}} = -2t(\cos k_x + \cos k_y) - 4t' \cos k_x \cos k_y. \quad (2)$$

The interaction term describes a d-wave weighted density-density interaction; $n_d(\mathbf{q}) = \sum_{\mathbf{k},\sigma} d_{\mathbf{k}} c^\dagger_{\mathbf{k}-(\mathbf{q}/2)\sigma} c_{\mathbf{k}+(\mathbf{q}/2)\sigma}$ with a d-wave form factor such as $d_{\mathbf{k}} = \cos k_x - \cos k_y$. The coupling strength $g(\mathbf{q})$ has a peak at $\mathbf{q} = 0$, that is, forward scattering dominates. This interaction drives a dPI at low temperatures as already studied in literature [11,12,17]. A crucial aspect of the present study lies in the third term in Eq. (1). This term is expressed as $-\mu_d \sum_{\mathbf{k},\sigma} (\cos k_x - \cos k_y) c^\dagger_{\mathbf{k}\sigma} c_{\mathbf{k}\sigma}$ and imposes an anisotropy of the nearest-neighbor hopping integral t between the x and y directions

$$t_x = t(1 + \mu_d/2t), \quad t_y = t(1 - \mu_d/2t). \quad (3)$$

A value of μ_d is controlled by applying a uniaxial pressure and a strain, and also by an orthorhombic crystal structure. μ_d may be interpreted as the d-wave chemical potential in the sense that it couples to the d-wave weighted charge density. Since the order parameter of the dPI is proportional to $n_d(\mathbf{0})$, μ_d is a conjugate field to that and plays an essential role to generate a Griffiths wing associated with the dPI.

The interaction term in Eq. (1) is obtained in microscopic models such as the t-J [9,18–20], Hubbard [10,21–25], and general models with central forces [26], and also from dipole-dipole interaction [27]. In fact those models exhibit a strong tendency toward the dPI at the low-energy scale, especially when the Fermi surface is close to saddle points around $(\pi,0)$ and $(0,\pi)$ where the d-wave form factor is enhanced. There can occur a competition with other instabilities such as superconductivity and magnetism in microscopic models, but Hamiltonian (1) does not contain interactions other than the dPI. Hence our model is regarded as a low-energy effective model of the dPI and considers a situation where the nematic tendency becomes dominant over the other ordering tendencies in realistic models; competing features among different instabilities are thus beyond the scope of the present study. Focusing on the nematic physics, we then wish to clarify the role of anisotropy in a rather general setup, independent of microscopic details. Although the interaction term might gain an anisotropic term especially for a large value of μ_d, we believe that the conceptional basis of Griffiths wings associated with nematicity is captured by Hamiltonian (1).

Hamiltonian (1) with $\mu_d = 0$, namely without anisotropy, was already studied in mean-field theory [11,12]. It was found [12] that the mean-field phase diagram of the dPI is determined by a single energy scale. As a result, there exist various universal ratios characterizing the phase diagram, which nicely capture experimental observations in $Sr_3Ru_2O_7$ [28,29]. The presence of momentum transfer $\mathbf{q}$ in the second term in Eq. (1) allows fluctuations around the mean-field solution. In an isotropic case ($\mu_d = 0$), it was shown that nematic order-parameter fluctuations change a first-order transition obtained in a mean-field theory into a continuous one when the fluctuations become sufficiently strong [30]; further stronger fluctuations can even destroy completely the nematic instability [31]. Nematic fluctuations close to a nematic quantum critical point lead to non-Fermi-liquid behavior [17,32,33]. It was also found that thermal nematic fluctuations near a nematic phase transition lead to a pronounced broadening of the quasiparticle peak with a strong momentum dependence characterized by the form factor $d^2_{\mathbf{k}}$, leading to a Fermi-arc-like feature [34]. A role of xy anisotropy ($\mu_d \neq 0$) was studied in the context of its strong enhancement due to the underling nematic correlations [9,23–25]. This feature was discussed to explain the strong anisotropy of magnetic excitation spectra [35–39] and the Nernst coefficient [40,41] in high-temperature superconductors. Except for these studies, a role of xy anisotropy in the nematic physics is poorly understood even in mean-field theory. This issue is addressed in terms of our Hamiltonian (1) including the effect of fluctuations on mean-field results.

We consider a phase diagram in the three-dimensional space spanned by μ, μ_d, and temperature T. The phase diagram is symmetric with respect to the axis of $\mu_d = 0$ and is almost symmetric with respect to the axis of $\mu = 0$ as long as t' is small. Hence we focus on the region of $\mu > 0$ and $\mu_d > 0$ by taking $t' = 0$. Since our conclusions do not depend on the magnitude of the interaction strength, we take $g = g(\mathbf{0}) = 1t$ in our numerical calculations. Considering previous studies in He^3-He^4 mixtures [13] and ferromagnetic systems [14], we may expect a wing structure emerging from a first-order transition of the dPI by applying the field μ_d. The upper edge of the wing is a critical end line (CEL), which is determined by the condition

$$\frac{\partial \omega}{\partial \phi} = \frac{\partial^2 \omega}{\partial \phi^2} = \frac{\partial^3 \omega}{\partial \phi^3} = 0, \quad (4)$$

where ω is the Gibbs free energy per lattice site and ϕ is the order parameter of the dPI. Below, all quantities of dimension of energy are presented in units of t.

III. MEAN-FIELD ANALYSIS

We first study Hamiltonian (1) in a mean-field theory. The interaction term is decoupled by introducing the order parameter

$$\phi = g n_d(\mathbf{0})/N, \quad (5)$$

where $g = g(\mathbf{0}) > 0$. The mean-field Hamiltonian then reads

$$H_{MF} = \sum_{\mathbf{k},\sigma} \xi_{\mathbf{k}} c^\dagger_{\mathbf{k}\sigma} c_{\mathbf{k}\sigma} + \frac{N}{2g}\phi^2, \quad (6)$$

with the renormalized band

$$\xi_{\mathbf{k}} = \epsilon^0_{\mathbf{k}} - \mu - (\phi + \mu_d) d_{\mathbf{k}}. \quad (7)$$

Obviously the conjugate field μ_d breaks xy symmetry and plays the same role as the order parameter ϕ. It is straightforward to obtain the free energy

$$\omega(\phi) = -\frac{2T}{N} \sum_{\mathbf{k}} \ln(1 + e^{-\xi_{\mathbf{k}}/T}) + \frac{1}{2g}\phi^2 \quad (8)$$

and we solve Eq. (4) numerically.

Figure 1(a) is a schematic mean-field phase diagram. At zero anisotropy ($\mu_d = 0$) the dPI occurs via a first-order

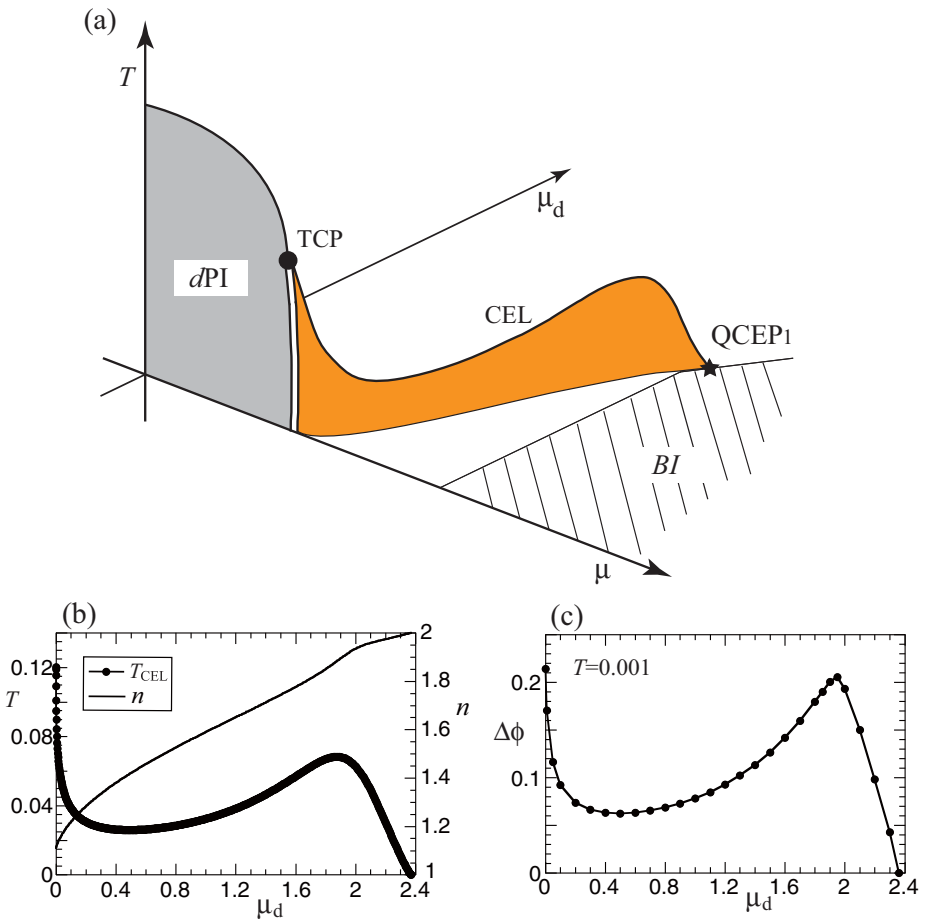

FIG. 1. (Color online) Mean-field results. (a) Schematic phase diagram in the space spanned by μ, μ_d, and T. At $\mu_d = 0$ the dPI occurs around Van Hove filling, from which μ is measured. The transition is of second order at high T (solid line) and of first order at low T (double line). The solid circle denotes the TCP. The BI state is realized in the striped region. The wing (colored in orange) stands almost vertically on the plane of μ and μ_d close to Van Hove filling and vanishes at the QCEP_1; the index 1 implies that the system is almost one dimensional. The upper edge of the wing (solid line) is a CEL. (b) Temperature of the CEL (T_{CEL}) as a function of μ_d; The wing is projected on the plane of μ_d and T. The electron density at T_{CEL} is also plotted. (c) Jump of the nematic order parameter across the wing at $T = 0.001$.

transition at low T as already found in previous studies [11,12]. With increasing μ, the band is eventually filled up and the band insulating (BI) state is realized in the striped region. Its phase boundary is given by $\mu = 4t$ for $\mu_d < 2$ and $\mu = 2\mu_d$ for $\mu_d > 2$ [42]. A wing emerges from the first-order line and extends to a region of a finite μ_d. The wing stands nearly vertically on the plane of μ_d and μ plane, and evolves close to Van Hove filling on that plane. To see the wing structure more closely, we project the CEL on the plane of μ_d and T in Fig. 1(b). The temperature of the CEL, T_{CEL}, is rapidly suppressed by applying the anisotropy μ_d, but does not go to zero. It recovers to form a broad peak around $\mu_d = 2$ and eventually vanishes when it touches the BI phase, leading to a quantum critical end point (QCEP) there. In fact, the electron density becomes two at the QCEP as seen in Fig. 1(b). When the system crosses the wing, the nematic order parameter exhibits a jump, leading to a metanematic transition. Such a jump, $\Delta\phi$, is plotted in Fig. 1(c) along the bottom of the wing as a function of μ_d. The magnitude of the jump exhibits behavior similar to T_{CEL}. It is interesting that $\Delta\phi$ around $\mu_d = 2$ becomes comparable to that at $\mu_d = 0$ in spite of the presence of a large external anisotropy.

Figure 1 can be understood in terms of the d-wave weighted density of states, $N_d(\mu) = \frac{1}{N}\sum_{\mathbf{k}} d_{\mathbf{k}}^2 \delta(\xi_{\mathbf{k}})$. This quantity appears in the second condition in Eq. (4), i.e., $\frac{\partial^2\omega}{\partial\phi^2} = 0$, and diverges at Van Hove filling unless the d-wave form factor vanishes at the saddle points. One can easily check that Eq. (4) is fulfilled close to such Van Hove filling, leading to the Griffiths wing there. While the field μ_d modifies a band structure as Eq. (3), the saddle points of the noninteracting band dispersion remain at $(\pi,0)$ and $(0,\pi)$ as long as $\mu_d < 2$. However, for $\mu_d > 2$, the saddle points shift to (π,π) and $(0,0)$. Around $\mu_d = 2$, therefore, the band becomes very flat, yielding a substantial enhancement of the density of states. This is the reason why T_{CEL} as well as $\Delta\phi$ exhibits a peak around $\mu_d = 2$; the peak position is slightly deviated from $\mu_d = 2$ because of the presence of a finite order parameter ϕ. Since the saddle points (π,π) and $(0,0)$ do not contribute to $N_d(\mu)$ because the d-wave form factor $d_{\mathbf{k}}$ vanishes there, T_{CEL} is suppressed for $\mu_d > 2$ and ultimately vanishes near the band edge. Since μ_d is very large close to the QCEP_1, the system is almost one dimensional [43]. Therefore we find a remarkable property that the Griffiths wing interpolates between a two- and (effectively) one-dimensional system by controlling the anisotropy.

IV. EFFECT OF ORDER-PARAMETER FLUCTUATIONS

In a mean-field theory we pick up the component with $\mathbf{q} = \mathbf{0}$ in Hamiltonian (1) [see also Eq. (5)]. Contributions from a finite $\mathbf{q}$ describe order-parameter fluctuations around the mean-field results. We address such fluctuation effects on the mean-field phase diagram. Since the Griffiths wing is realized near the Van Hove singularity, a usual polynomial expansion of the order-parameter potential [44] is not valid

there. To circumvent such a problem, we employ a functional renormalization-group (fRG) scheme [45]. This scheme allows us to analyze fluctuations without any expansion of the potential [46] and was successfully applied to studies of fluctuation effects of the dPI in an isotropic case ($\mu_d = 0$) [30,31].

We use a path-integral formalism and follow a usual procedure to derive an order-parameter action [44]. That is, we first decouple the fermionic interaction in Eq. (1) by introducing a Hubbard-Stratonovich field associated with the fluctuating order parameter of the dPI and then integrate fermionic degrees of freedom. Because we are interested in low-energy, long-wavelength fluctuations of the dPI, we retain the leading momentum and frequency dependencies of the two-point function and neglect such dependencies in high-order vertex functions. The resulting order-parameter action becomes

$$S[\phi] = \frac{1}{2}\sum_q{}' \left[\phi_q \left(A_0 \frac{|\omega_n|}{|\mathbf{q}|} + Z_0 \mathbf{q}^2\right)\phi_{-q}\right] + \mathcal{U}[\phi], \quad (9)$$

where ϕ_q with $q = (\mathbf{q},\omega_n)$ denotes the momentum representation of the order-parameter field ϕ and $\omega_n = 2\pi n T$ with integer n denotes the bosonic Matsubara frequencies. The approximation scheme of our action (9) corresponds to the next-leading order of derivative expansion. Hence the momenta and frequencies contributing to the action $S[\phi]$ should be restricted by the cutoff Λ_0 to the region $\frac{A_0|\omega_n|}{Z_0|\mathbf{q}|} + \mathbf{q}^2 \leqslant \Lambda_0^2$, as emphasized by adding the prime in the summation in Eq. (9). In the fermionic representation, Λ_0 may be related to the maximal momentum transfer allowed by the interaction in the second term in Hamiltonian (1). If Λ_0 is set to be zero, the action (9) reproduces the mean-field theory. Physically, therefore, the value of Λ_0 controls the strength of order-parameter fluctuations. The effective potential $\mathcal{U}[\phi]$ is given by $\mathcal{U}[\phi] = \int_0^{1/T} d\tau \int d^2\mathbf{r}\, U[\phi(\mathbf{r},\tau)]$, where $U(\phi)$ is equal to the mean-field potential [Eq. (8)] and we do not expand it in powers of ϕ, in contrast to the usual case [44].

We carry out calculations in the one-particle irreducible scheme of the fRG by computing the flow of the effective action $\Gamma^\Lambda[\phi]$ in the presence of an infrared cutoff Λ [45,47]. In this scheme $\Gamma^\Lambda[\phi]$ interpolates between the bare action $S[\phi]$ [Eq. (9)] at the ultraviolet cutoff Λ^{UV} and the thermodynamic potential $\omega(\phi)$ in the limit of $\Lambda \to 0$. Its evolution is given by the functional exact flow equation [46],

$$\partial_\Lambda \Gamma^\Lambda[\phi] = \frac{1}{2}\mathrm{tr}\frac{\partial_\Lambda R^\Lambda}{\Gamma_2^\Lambda[\phi] + R^\Lambda}, \quad (10)$$

where R^Λ is a regulator and $\Gamma_2^\Lambda[\phi] = \delta^2\Gamma^\Lambda[\phi]/\delta\phi^2$. We choose a Litim-type regulator [48] used in previous works [30,31]: $R^\Lambda = [Z(\Lambda^2 - \mathbf{q}^2) - A\frac{|\omega_n|}{|\mathbf{q}|}]\theta(Z(\Lambda^2 - \mathbf{q}^2) - A\frac{|\omega_n|}{|\mathbf{q}|})$. A form of $\Gamma^\Lambda[\phi]$ is highly complicated and we parametrize it as

$$\Gamma^\Lambda[\phi] = \frac{1}{2}\sum_q{}' \left[\phi_q \left(A^\Lambda \frac{|\omega_n|}{|\mathbf{q}|} + Z^\Lambda \mathbf{q}^2\right)\phi_{-q}\right] + \mathcal{U}^\Lambda[\phi], \quad (11)$$

the same functional form as Eq. (9). We allow flows of Z^Λ and $\mathcal{U}^\Lambda$, but discard the flow of A^Λ, which is of minor importance [49] and is assumed to be $A^\Lambda = A_0$. Inserting Eq. (11) into Eq. (10) and evaluating the resulting equations for uniform fields, we obtain the flow equations of Z^Λ and U^Λ; their derivations contain technical details and thus are left to the Appendix. By solving these flow equations numerically by reducing Λ from Λ^{UV} to zero, we can determine the thermodynamic potential $\omega(\phi)$, which carries over the effect of nematic order-parameter fluctuations. To determine the Griffiths wing, we then search for a solution of Eq. (4) in the three-dimensional space spanned by μ, μ_d, and T. All these computations are performed numerically and require highly accurate numerics, otherwise higher-order derivatives of the free energy, which are contained in Eq. (4), would not become smooth enough to conclude a phase diagram.

Figure 2(a) is a schematic phase diagram in the presence of order-parameter fluctuations. The dPI phase diagram at zero anisotropy is slightly suppressed by fluctuations, but retains essentially the same features as the mean-field result. Applying the anisotropy μ_d, the CEL is rapidly suppressed, leading to a tiny wing terminating at a QCEP_2. We then have a crossover region depicted by the dashed line. The order parameter of the dPI shows a rapid change, but without a jump, by crossing the dashed line. With further increasing μ_d, another wing emerges with two QCEPs. While the Griffiths wing is broken up into two separate pieces by fluctuations, the two wings are connected via a crossover line [dashed line in Fig. 2(a)] as reminiscence of a single Griffiths wing in the absence of fluctuations [Fig. 1(a)].

These results may be understood as originating from a unique feature of the mean-field result, namely the suppression of T_{CEL} in an intermediate region of μ_d in Fig. 1(b). Given that ϕ enters the renormalized dispersion Eq. (7), it is easily expected that fluctuations of ϕ blur the Van Hove singularity and yield the suppression of the density of states. Consequently, relatively low T_{CEL} obtained in the mean-field theory is easily suppressed to become zero, leading to the breaking of the Griffiths wing.

In Figs. 2(b) and 2(c) two Griffiths wings are projected on the plane of μ_d and T. The results are shown for several choices of the cutoff Λ_0, which controls the strength of fluctuations as introduced in Eq. (9); a larger Λ_0 means stronger fluctuations. When Λ_0 becomes larger, the CELs are suppressed more as expected. This suppression is, however, quite remarkable. To quantify the suppression, we consider the critical external anisotropy, $\Delta t_c/t = \frac{t_x - t_y}{t_x + t_y} = \mu_d/2t$, to obtain a QCEP. We plot $\Delta t_c/t$ in Fig. 2(d) as a function of the ratio of the tricritical temperature and its mean-field value ($T_{\mathrm{TCP}}/T_{\mathrm{TCP}}^{\mathrm{MF}}$) as the strength of fluctuations. We see that when T_{TCP} is suppressed by fluctuations, for example, by half, a very small anisotropy ($\Delta t_c/t \approx 0.01$) is sufficient to yield a QCEP. Furthermore the strength of fluctuations to realize the QCEP is weak in the sense that the dPI phase diagram at $\mu_d = 0$ is still well captured by mean-field theory. Therefore we conclude that the Griffiths wing is very sensitive to fluctuations and the QCEP_2 can be reached with a weak anisotropy even though the transition is of first order at zero anisotropy. This is sharply different from the mean-field result [Fig. 1(a)] where a QCEP can be reached with a very strong anisotropy, i.e., $\Delta t_c/t \approx 1.2$ for $T_{\mathrm{TCP}}/T_{\mathrm{TCP}}^{\mathrm{MF}} = 1$.

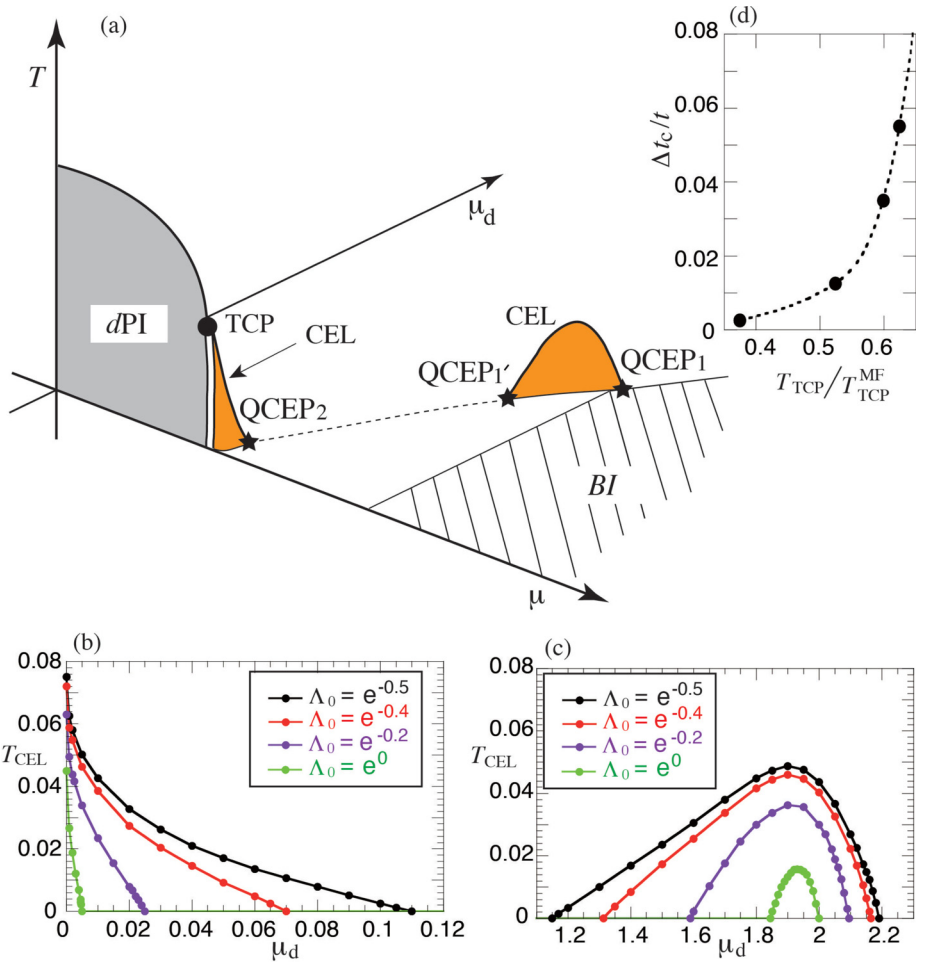

FIG. 2. (Color online) Results in the presence of weak nematic order-parameter fluctuations. (a) Schematic phase diagram. The dPI phase is slightly suppressed by fluctuations. The wing obtained in Fig. 1(a) is broken into two pieces: one tiny wing close to $\mu_d = 0$ and the other wing for a large μ_d. The indices of $QCEP_2$ and $QCEP_{1'}$ imply that the system can be regarded to be two- and quasi-one-dimensional, respectively, at the QCEP. The dashed line corresponds to a crossover. The BI phase is assumed to be the same as the mean-field result. (b),(c) The wings are projected on the plane of μ_d and T for several choices of the cutoff Λ_0. (d) The critical anisotropy of the hopping integral to obtain the $QCEP_2$ as a function of the ratio of the tricritical temperature and its mean-field value.

V. DISCUSSIONS

Usually mean-field theory is powerful to discuss actual materials at least about qualitative features. However, the Griffiths wing turns out to be sensitive even to weak fluctuations, leading to the phase diagram (Fig. 2) qualitatively different from the mean-field phase diagram (Fig. 1). Since we may always have at least weak fluctuations of the order parameter in actual materials, Fig. 2 is expected to be more realistic than Fig. 1. Hence we bear Fig. 2 in mind and discuss relevance to various systems as well as theoretical implications for future studies.

Cuprates. Neutron-scattering experiments showed that the magnetic excitation spectrum becomes anisotropic in momentum space. The anisotropy observed in $YBa_2Cu_3O_{6.85}$ and $YBa_2Cu_3O_{6.6}$ [35,36] is relatively weak and is well captured in terms of competition of the tendency toward the dPI and pairing correlations [38]. For $YBa_2Cu_3O_{6.45}$, however, Ref. [37] reported a very strong anisotropy, which could not be interpreted in the same theory as Ref. [38]. Instead two different theories were proposed: one invoking the presence of a nematic quantum critical point [50] and the other invoking a dominant nematic tendency over the pairing tendency [39]. The point is that the observed anisotropy seems to suddenly change by crossing the oxygen concentration around 6.45.

Microscopic models of cuprates such as the t-J and Hubbard models exhibit the dPI tendency as shown by various approximation schemes: slave-boson mean-field theory [9], exact diagonalization [18], variational Monte Carlo [19], a large-N expansion [20], dynamical mean-field theory for clusters [23,24], and dynamical cluster quantum Monte Carlo approximation [25]. Furthermore our low-energy effective interaction [the second term in Eq. (1)] can be obtained from those microscopic models [9,10,21]; for example, our interaction term is given by $g(\mathbf{q}) = 3J/8$ at a bare level in the t-J model. In fact, the t-J model [9,19,20] exhibits a nematic tendency very similar to the present results (Figs. 1 and 2 for $\mu_d = 0$): the nematicity in the t-J model is strongly enhanced upon approaching half filling, which corresponds to Van Hove filling of the spinon dispersion in the slave-boson mean-field theory [51]. Although the microscopic models for cuprates contain interactions other than the nematic channel, our model assumes a situation where the nematic tendency becomes dominant over other tendencies. This situation actually occurs in a region around oxygen concentration 6.45 in Y-based cuprates. Hence we expect that the present low-energy theory can give some insight into the nematicity observed in cuprates.

Superconducting samples of Y-based cuprates have an intrinsic xy anisotropy coming from the CuO chain structure and its anisotropy is estimated around $\mu_d = 0.03$–0.04 [38]. Hence Y-based cuprates are located along the axis of a small μ_d in Fig. 2(a); the density at $\mu = 0$ in that figure corresponds to half filling in cuprates. With decreasing μ (hole picture), namely decreasing the oxygen concentration, the system can cross the tiny wing or pass close to the $QCEP_2$, which may explain a sudden change of the anisotropy observed

in the magnetic excitation spectrum [37]. In this context, it is interesting to explore a possibility that the presence of a nematic quantum critical point assumed in previous studies [50,52] is connected with the $QCEP_2$.

In reality, antiferromagnetic Mott insulators are realized at half filling in cuprates. Strong correlation effects associated with the Mott transition will then yield an enhancement of the density of states upon approaching the half filling, which contributes to an enhancement of the nematic tendency [9,19,20,23–25]. Because of these additional features in cuprates, it may be thoughtful to emphasize the proximity to the Mott insulator, rather than the Van Hove singularity of the spinon dispersion [51], as an important factor to discuss the nematicity upon approaching half filling [37,53]. In fact, Van Hove filling in cuprates is usually emphasized in a heavily overdoped region [54]. Theoretical studies of the t-J model [9,20] predict a nematic instability also around such Van Hove filling and thus a Griffiths wing is expected there by applying xy anisotropy. The heavily overdoped region in cuprates, however, is not studied much experimentally.

Ruthenates. The strontium ruthenate $Sr_3Ru_2O_7$ exhibits an electronic nematic instability around a magnetic field 8 T [6]. The band structure calculations show six Fermi surfaces at zero magnetic field [55,56]. There is a two-dimensional Fermi surface very close to the momenta $(\pi,0)$ and $(0,\pi)$, which contribute to the large density of states near the Fermi energy. Hence focusing on such a two-dimensional band near Van Hove filling, the nematic instability in $Sr_3Ru_2O_7$ is frequently discussed in terms of a one-band model. The interaction term in Hamiltonian (1) is employed in various theoretical studies for $Sr_3Ru_2O_7$ [57–63]. In spite of such a simple model, it turns out that the model captures major aspects of the experimental phase diagram except for a slope of the first-order transition [28,64]. Although the Zeeman field is not considered in the present theory, it simply splits the Fermi surfaces of the spin-up and spin-down band and then tunes the Fermi surface of either spin closer to Van Hove filling, a very similar role to the chemical potential. In fact, explicit calculations including the Zeeman field confirm this consideration [28,29,57,64]. Hence we interpret the chemical potential μ in Fig. 2(a) as a magnetic field h in $Sr_3Ru_2O_7$; $\mu = 0$ in our figure may correspond to $h = 7.95$ T in that material and our phase boundaries of the dPI at $T = 0$ correspond to $h = 7.85$ and 8.1 T. Since $Sr_3Ru_2O_7$ has a tetragonal structure, the system is located along the axis of $\mu_d = 0$ in our phase diagram. Therefore, on the basis of the present study (Fig. 2), we expect an emergence of a tiny Griffiths wing close to $\mu_d = 0$ by applying a strain along the x or y direction in $Sr_3Ru_2O_7$ [65]. If the system gains an anisotropy of in-plane lattice constants by x%, the anisotropy of t is expected around $3.5x$% when hybridization between the Ru d and O p states is a major contribution to t [66]. Since a required anisotropy of t to reach a QCEP can become very small [see Fig. 2(d)], not only the rapid drop of the CEL, but also the QCEP can be observed in experiments.

There are other theories for $Sr_3Ru_2O_7$, focusing on a metamagnetic transition [67,68], occupation differences between d_{yz} and d_{zx} orbitals [69,70], and inhomogeneous magnetic phases [71]. Although these studies propose a mechanism different from the electronic nematic instability, Van Hove singularities play an important role also in those theories. The proximity to the Van Hove singularity is directly observed by angle-resolved photoemission spectroscopy [72] and is thus likely a key factor to discuss $Sr_3Ru_2O_7$.

Quasi-one-dimensional metals. We have revealed that the Griffiths wing interpolates between a two- and one-dimensional system. In fact, a piece of the broken Griffiths wings is realized also for a strong anisotropy in Figs. 2(a) and 2(c). Such a strong anisotropy is intrinsically realized in quasi-one-dimensional metals. In this case, when the system is located close to Van Hove filling, our theory predicts that the anisotropy of the electronic system can change dramatically by controlling a uniaxial pressure or carrier density. Although we are not aware of experiments discussing such a phenomenon, there are theoretical works reporting it in a different context [73] and their metanematic transition can be interpreted as originating from a Griffiths wing. Since theoretically various microscopic interactions can generate an attractive interaction of the dPI [9,10,21,26,27] and experimentally xy anisotropy of physical quantities in an already strongly anisotropic system was not likely recognized as something related to nematicity in the past, we may reasonably wait for further experiments.

Cold atom systems. Each condensed-matter system is characterized by a certain value of μ_d, which is determined by an intrinsic property of the material such as a crystal structure and thus cannot be changed much externally. However, μ_d is fully tunable for optical lattices in a cold atom system [73,74] by changing the strength of laser beams between the x and y direction. One may employ cold fermions with a large dipolar moment and align the dipole along the z direction. Dipolar interaction then yields a repulsive interaction between fermions, which leads to an attractive interaction of the dPI, i.e., the second term in Eq. (1) [21,27]. A Griffiths wing is then expected near Van Hove filling at temperatures well below the Fermi energy [Fig. 2(a)]. Such low temperatures are now accessible in experiments [75].

Iron-based superconductors. There are intensive discussions about orthorhombicity and nematicity [5,76] in terms of spin [77], orbital [78,79], and both [80] degrees of freedom. However, the nematic transition in iron-based superconductors usually occurs through a continuous phase transition and there is not evidence of a TCP associated with a nematic transition. Hence the present theory may not be applicable to iron-based superconductors.

Anomalous ground state. Our obtained results (Fig. 2) contain interesting insights into electronic nematicity and will likely promote further theoretical studies. A non-Fermi-liquid ground state is stabilized at a quantum critical point of the dPI [17,32,33]. It is plausible to expect an anomalous ground state also at a QCEP of the dPI. In an intermediate region between the $QCEP_2$ and $QCEP_{1'}$, the dashed line in Fig. 2(a), quantum fluctuations completely wash out the wing even close to Van Hove filling. If the system remains a Fermi liquid there, the density of states would diverge at Van Hove filling. We would then expect a Griffiths wing there because our Hamiltonian (1) has an attractive interaction of the dPI. However, we have obtained a crossover around the dashed line in Fig. 2(a). This consideration hints a possible non-Fermi-liquid ground state at Van Hove filling; the same conclusion was obtained also by Dzyaloshinskii in a different context [81]. Therefore xy anisotropy can lead to an anomalous ground state in a

wide parameter space spanned by μ and μ_d, even though the quantum phase transition is a first order at zero anisotropy.

VI. CONCLUSIONS

Electronic nematic order couples directly to xy anisotropy. The anisotropy can be controlled by applying a uniaxial pressure and a strain. Moreover, actual materials often contain intrinsic anisotropy due to a crystal structure such as orthorhombicity. The present theory addresses such a situation in a rather general setup by including the d-wave chemical potential μ_d in a low-energy effective Hamiltonian of an electronic nematic instability [see Eq. (1)]. Although the nematic physics is frequently discussed in a two-dimensional system, the present theory shows that the nematic physics is important also in an anisotropic system. We have shown that the Griffiths wing associated with the nematicity interpolates between a two- and (nearly) one-dimensional system by changing the anisotropy (Figs. 1 and 2). In fact, a recent theoretical work [73] reports a metanematic phenomenon in an anisotropic system, which can be interpreted as coming from the Griffiths wing. The Griffiths wing of the nematicity is found to be quite unique in the sense that it exhibits a nonmonotonic temperature dependence (Fig. 1), in sharp contrast to the cases of He^3-He^4 mixtures [13] and ferromagnetic systems [14–16]. The Griffiths wing turns out to be very sensitive to nematic order-parameter fluctuations, leading to a phase diagram (Fig. 2) topologically different from the mean-field phase diagram: a QCEP close to zero anisotropy, a crossover region, and a broken Griffiths wing terminated with two QCEPs in a strong anisotropy. This suggests that even if fluctuations are relatively weak in the sense that the phase diagram is still well captured by mean-field theory at zero anisotropy, fluctuation effects can be dramatic once xy anisotropy is introduced. Hence the effect of fluctuations is definitely important to the Griffiths wing. Given that order-parameter fluctuations are present to a greater or lesser extent in actual materials, our Fig. 2 is expected to be more realistic than Fig. 1. Not only at three QCEPs, but also in the crossover region, the ground state may feature non-Fermi-liquid behavior. This possibility is very interesting since a non-Fermi-liquid state can extend in a wide parameter space at zero temperature. We hope that the present theory serves as a fundamental basis of the nematic physics in various materials such as high-T_c cuprates, double-layered ruthenates, quasi-one-dimensional metals, and cold atoms, and will promote further theoretical studies.

ACKNOWLEDGMENTS

The author appreciates very much insightful and valuable discussions with K. Aikawa, F. Benitez, A. Eberlein, T. Enss, A. Greco, N. Hasselmann, P. Jakubczyk, A. Katanin, W. Metzner, M. Nakamura, B. Obert, and S. Takei. Support by the Alexander von Humboldt Foundation (Germany) and a Grant-in-Aid for Scientific Research from Monkasho (Japan) is also greatly appreciated.

APPENDIX

In this Appendix we present technical details of our fRG framework.

Our formalism of the fRG partly overlaps with previous works [30,31], which studied how nematic fluctuations change the mean-field phase diagram for $\mu_d = 0$. Compared with previous calculations [30,31], we did the following extension: (i) Introduction of two cutoffs, one is the physical cutoff Λ_0 which gives the upper cutoff to the summation in Eq. (9) as emphasized by adding the prime to the symbol Σ, and the other is the ultraviolet cutoff $\Lambda^{\rm UV}$ which is in principle infinite. In the previous formalism [30,31] $\Lambda^{\rm UV}$ was assumed to be identical to Λ_0. (ii) No additional approximations to compute the right-hand side of flow equations, that is, we take account of quantum fluctuations in the anomalous dimension $\eta = -\frac{\partial \ln Z}{\partial \ln \Lambda}$, the contribution from the term $\frac{\partial Z}{\partial \Lambda}$, and an additional term coming from the momentum derivative of the regular for the flow of Z.

The resulting flow equations become different from those in Refs. [30] and [31]:

$$\Lambda \partial_\Lambda U(\phi) = \frac{T}{4\pi} \frac{1}{1+\frac{U''}{Z\Lambda^2}} \left\{ \frac{2-\eta}{2} \left[\hat{\Lambda}^2 + 2 \sum_{n=1}^{n_{\rm max}} \left(\hat{q}_2^2 - \hat{q}_1^2 \right) \right] + \frac{\eta}{4\Lambda^2} \left[\hat{\Lambda}^4 + 2 \sum_{n=1}^{n_{\rm max}} \left(\hat{q}_2^4 - \hat{q}_1^4 \right) \right] \right\}, \tag{A1}$$

$$\Lambda \partial_\Lambda Z = -\eta Z, \tag{A2}$$

and

$$\eta = \begin{cases} \dfrac{\dfrac{T}{4\pi} \dfrac{(U''')^2}{Z^3 \Lambda^6 (1+\frac{U''}{Z\Lambda^2})^4} \left[\Lambda^2 + 3 \sum_{n=1}^{n_{\rm max}} (\hat{q}_2^2 - \hat{q}_1^2) \right]}{1 + \dfrac{T}{8\pi} \dfrac{(U''')^2}{Z^3 \Lambda^6 (1+\frac{U''}{Z\Lambda^2})^4} \sum_{n=1}^{n_{\rm max}} (\hat{q}_2^2 - \hat{q}_1^2) \left[4 - \dfrac{3}{\Lambda^2} (\hat{q}_2^2 + \hat{q}_1^2) \right]} & \text{for } \Lambda \leqslant \Lambda_0, \\ 0 & \text{for } \Lambda > \Lambda_0. \end{cases} \tag{A3}$$

η is evaluated at a position where $U(\phi)$ has the global minimum; $U''(U''')$ denotes the second (third) derivative with respect to ϕ; $n_{\rm max}$ is the maximum Matsubara frequency contributing to the flow equations and is given by $n_{\rm max} = [\frac{Z\hat{\Lambda}^3}{3\pi\sqrt{3}A_0 T}]$; $\hat{q}_1 (>0)$ and $\hat{q}_2 (\geqslant \hat{q}_1)$ are real roots of the equation

$$q^3 - \hat{\Lambda}^2 q + \frac{A_0}{Z} |\omega_n| = 0; \tag{A4}$$

and

$$\hat{\Lambda} = \begin{cases} \Lambda & \text{for} \quad \Lambda \leqslant \Lambda_0, \\ \Lambda_0 & \text{for} \quad \Lambda > \Lambda_0. \end{cases} \tag{A5}$$

We solve the differential equations (A1) and (A2) numerically by reducing Λ from $\Lambda^{\rm UV}$ to zero; the initial condition is given by the bare action Eq. (9). Since we cannot set $\Lambda^{\rm UV} = \infty$ numerically, we first did calculations for various choices of large $\Lambda^{\rm UV}$ and checked that our conclusions do not depend on the value of $\Lambda^{\rm UV}(\geqslant \Lambda_0)$. In addition, our conclusions also do not depend on a precise choice of A_0 and Z_0. We took $\Lambda^{\rm UV} = \Lambda_0$, $A_0 = 1$, and $Z_0 = 10$ in Fig. 2.

[1] M. P. Lilly, K. B. Cooper, J. P. Eisenstein, L. N. Pfeiffer, and K. W. West, Phys. Rev. Lett. **82**, 394 (1999).
[2] R. R. Du, D. C. Tsui, H. L. Stormer, L. N. Pfeiffer, K. W. Baldwin, and K. W. West, Solid State Commun. **109**, 389 (1999).
[3] S. A. Kivelson, I. P. Bindloss, E. Fradkin, V. Oganesyan, J. M. Tranquada, A. Kapitulnik, and C. Howald, Rev. Mod. Phys. **75**, 1201 (2003).
[4] M. Vojta, Adv. Phys. **58**, 699 (2009).
[5] I. R. Fisher, L. Degiorgi, and Z. X. Shen, Rep. Prog. Phys. **74**, 124506 (2011).
[6] A. P. Mackenzie, J. A. N. Bruin, R. A. Borzi, A. W. Rost, and S. A. Grigera, Physica C **481**, 207 (2012).
[7] R. Okazaki, T. Shibauchi, H. J. Shi, Y. Haga, T. D. Matsuda, E. Yamamoto, Y. Onuki, H. Ikeda, and Y. Matsuda, Science **331**, 439 (2011).
[8] J.-H. Chu, H.-H. Kuo, J. G. Analytis, and I. R. Fisher, Science **337**, 710 (2012).
[9] H. Yamase and H. Kohno, J. Phys. Soc. Jpn. **69**, 332 (2000); **69**, 2151 (2000).
[10] C. J. Halboth and W. Metzner, Phys. Rev. Lett. **85**, 5162 (2000).
[11] I. Khavkine, C.-H. Chung, V. Oganesyan, and H.-Y. Kee, Phys. Rev. B **70**, 155110 (2004).
[12] H. Yamase, V. Oganesyan, and W. Metzner, Phys. Rev. B **72**, 035114 (2005).
[13] R. B. Griffiths, Phys. Rev. Lett. **24**, 715 (1970).
[14] D. Belitz, T. R. Kirkpatrick, and J. Rollbühler, Phys. Rev. Lett. **94**, 247205 (2005).
[15] H. Kotegawa, V. Taufour, D. Aoki, G. Knebel, and J. Flouqet, J. Phys. Soc. Jpn. **80**, 083703 (2011).
[16] D. Aoki, T. Combier, V. Taufour, T. D. Matsuda, G. Knebel, H. Kotegawa, and J. Flouquet, J. Phys. Soc. Jpn. **80**, 094711 (2011).
[17] W. Metzner, D. Rohe, and S. Andergassen, Phys. Rev. Lett. **91**, 066402 (2003).
[18] A. Miyanaga and H. Yamase, Phys. Rev. B **73**, 174513 (2006).
[19] B. Edegger, V. N. Muthukumar, and C. Gros, Phys. Rev. B **74**, 165109 (2006).
[20] M. Bejas, A. Greco, and H. Yamase, Phys. Rev. B **86**, 224509 (2012).
[21] B. Valenzuela and M. A. H. Vozmediano, Phys. Rev. B **63**, 153103 (2001).
[22] I. Grote, E. Körding, and F. Wegner, J. Low Temp. Phys. **126**, 1385 (2002); V. Hankevych, I. Grote, and F. Wegner, Phys. Rev. B **66**, 094516 (2002).
[23] S. Okamoto and N. Furukawa, Phys. Rev. B **86**, 094522 (2012).
[24] S. Okamoto, D. Sénéchal, M. Civelli, and A.-M. S. Tremblay, Phys. Rev. B **82**, 180511(R) (2010).
[25] S.-Q. Su and T. A. Maier, Phys. Rev. B **84**, 220506(R) (2011).
[26] J. Quintanilla, M. Haque, and A. J. Schofield, Phys. Rev. B **78**, 035131 (2008).
[27] C. Lin, E. Zhao, and W. V. Liu, Phys. Rev. B **81**, 045115 (2010).
[28] H. Yamase, Phys. Rev. B **76**, 155117 (2007).
[29] H. Yamase, Phys. Rev. B **87**, 195117 (2013).
[30] P. Jakubczyk, W. Metzner, and H. Yamase, Phys. Rev. Lett. **103**, 220602 (2009).
[31] H. Yamase, P. Jakubczyk, and W. Metzner, Phys. Rev. B **83**, 125121 (2011).
[32] V. Oganesyan, S. A. Kivelson, and E. Fradkin, Phys. Rev. B **64**, 195109 (2001).
[33] M. Garst and A. V. Chubukov, Phys. Rev. B **81**, 235105 (2010).
[34] H. Yamase and W. Metzner, Phys. Rev. Lett. **108**, 186405 (2012).
[35] V. Hinkov, S. Pailhès, P. Bourges, Y. Sidis, A. Ivanov, A. Kulakov, C. T. Lin, D. Chen, C. Bernhard, and B. Keimer, Nature (London) **430**, 650 (2004).
[36] V. Hinkov, P. Bourges, S. Pailhès, Y. Sidis, A. Ivanov, C. D. Frost, T. G. Perring, C. T. Lin, D. P. Chen, and B. Keimer, Nat. Phys. **3**, 780 (2007).
[37] V. Hinkov, D. Haug, B. Fauqué, P. Bourges, Y. Sidis, A. Ivanov, C. Bernhard, C. T. Lin, and B. Keimer, Science **319**, 597 (2008).
[38] H. Yamase and W. Metzner, Phys. Rev. B **73**, 214517 (2006).
[39] H. Yamase, Phys. Rev. B **79**, 052501 (2009).
[40] R. Daou, J. Chang, D. LeBoeuf, O. Cyr-Choinière, F. Laliberté, N. Doiron-Leyraud, B. J. Ramshaw, R. Liang, D. A. Bonn, W. H. Hardy *et al.*, Nature (London) **463**, 519 (2010).
[41] A. Hackl and M. Vojta, Phys. Rev. B **80**, 220514(R) (2009).
[42] In the presence of a small t' ($|t'/t| < 0.5$), the BI is realized for $\mu = 4(t - t')$ for $0 < \mu_d < 2(t - 2t')$ and $\mu = 2(\mu_d + 2t')$ for $\mu_d > 2(t - 2t')$.
[43] If t' is included, the system always allows a hopping along the diagonal direction. Hence the anisotropy of $\mu_d \approx 2$ does not necessarily mean that the system becomes fully one dimensional.
[44] J. A. Hertz, Phys. Rev. B **14**, 1165 (1976).
[45] W. Metzner, M. Salmhofer, C. Honerkamp, V. Meden, and K. Schönhammer, Rev. Mod. Phys. **84**, 299 (2012).
[46] C. Wetterich, Phys. Lett. B **301**, 90 (1993).
[47] Λ is a quantity independent of Λ_0. Λ moves from $\Lambda^{\rm UV}$ to zero whereas Λ_0 is a fixed quantity introduced in Eq. (9).
[48] D. F. Litim, Phys. Rev. D **64**, 105007 (2001).

[49] P. Jakubczyk, P. Strack, A. A. Katanin, and W. Metzner, Phys. Rev. B **77**, 195120 (2008).
[50] E.-A. Kim, M. J. Lawler, P. Oreto, S. Sachdev, E. Fradkin, and S. A. Kivelson, Phys. Rev. B **77**, 184514 (2008).
[51] P. A. Lee, N. Nagaosa, and X.-G. Wen, Rev. Mod. Phys. **78**, 17 (2006).
[52] Y. Huh and S. Sachdev, Phys. Rev. B **78**, 064512 (2008).
[53] D. Haug, V. Hinkov, Y. Sidis, P. Bourges, N. B. Christensen, A. Ivanov, T. Keller, C. T. Lin, and B. Keimer, New J. Phys. **12**, 105006 (2010).
[54] A. Piriou, N. Jenkins, C. Berhod, I. Maggio-Aprile, and Ø. Fischer, Nat. Commun. **2**, 221 (2011).
[55] I. Hase and Y. Nishihara, J. Phys. Soc. Jpn. **66**, 3517 (1997).
[56] D. J. Singh and I. I. Mazin, Phys. Rev. B **63**, 165101 (2001).
[57] H.-Y. Kee and Y. B. Kim, Phys. Rev. B **71**, 184402 (2005).
[58] H. Doh, Y. B. Kim, and K. H. Ahn, Phys. Rev. Lett. **98**, 126407 (2007).
[59] C. Puetter, H. Doh, and H.-Y. Kee, Phys. Rev. B **76**, 235112 (2007).
[60] H. Yamase, Phys. Rev. Lett. **102**, 116404 (2009).
[61] H. Yamase, Phys. Rev. B **80**, 115102 (2009).
[62] A. F. Ho and A. J. Schofield, Europhys. Lett. **84**, 27007 (2008).
[63] M. H. Fischer and M. Sigrist, Phys. Rev. B **81**, 064435 (2010).
[64] H. Yamase and A. A. Katanin, J. Phys. Soc. Jpn. **76**, 073706 (2007).
[65] While an xy anisotropy is also generated by introducing a magnetic field along the x or y direction [6], the coupling to electrons is different from our anisotropic field of μ_d.
[66] W. A. Harrison, *Electronic Structure and the Properties of Solids* (Dover, New York, 1989).
[67] A. J. Millis, A. J. Schofield, G. G. Lonzarich, and S. A. Grigera, Phys. Rev. Lett. **88**, 217204 (2002).
[68] B. Binz and M. Sigrist, Europhys. Lett. **65**, 816 (2004).
[69] S. Raghu, A. Paramekanti, E-.A. Kim, R. A. Borzi, S. A. Grigera, A. P. Mackenzie, and S. A. Kivelson, Phys. Rev. B **79**, 214402 (2009).
[70] W.-C. Lee and C. Wu, Phys. Rev. B **80**, 104438 (2009).
[71] A. M. Berridge, A. G. Green, S. A. Grigera, and B. D. Simons, Phys. Rev. Lett. **102**, 136404 (2009).
[72] A. Tamai, M. P. Allan, J. F. Mercure, W. Meevasana, R. Dunkel, D. H. Lu, R. S. Perry, A. P. Mackenzie, D. J. Singh, Z.-X. Shen, and F. Baumberger, Phys. Rev. Lett. **101**, 026407 (2008).
[73] J. Quintanilla, S. T. Carr, and J. J. Betouras, Phys. Rev. A **79**, 031601(R) (2009); S. T. Carr, J. Quintanilla, and J. J. Betouras, Phys. Rev. B **82**, 045110 (2010).
[74] I. Bloch, J. Dalibard, and W. Zwerger, Rev. Mod. Phys. **80**, 885 (2008).
[75] K. Aikawa, A. Frisch, M. Mark, S. Baier, R. Grimm, and F. Ferlaino, Phys. Rev. Lett. **112**, 010404 (2014).
[76] R. M. Fernandes, A. V. Chubukov, and J. Schmalian, Nat. Phys. **10**, 97 (2014).
[77] R. M. Fernandes, L. H. VanBebber, S. Bhattacharya, P. Chandra, V. Keppens, D. Mandrus, M. A. McGuire, B. C. Sales, A. S. Sefat, and J. Schmalian, Phys. Rev. Lett. **105**, 157003 (2010).
[78] H. Kontani, T. Saito, and S. Onari, Phys. Rev. B **84**, 024528 (2011).
[79] W. Lv and P. Phillips, Phys. Rev. B **84**, 174512 (2011).
[80] S. Liang, A. Moreo, and E. Dagotto, Phys. Rev. Lett. **111**, 047004 (2013).
[81] I. Dzyaloshinskii, J. Phys. I France **6**, 119 (1996).